JOURNAL OF GEOPHYSICAL RESEARCH, VOL. 115, A00F11, doi:10.1029/2009JA014845, 2010

THEMIS analysis of observed equatorial electron distributions responsible for the chorus excitation

W. Li,[1] R. M. Thorne,[1] Y. Nishimura,[1,2] J. Bortnik,[1] V. Angelopoulos,[3] J. P. McFadden,[4] D. E. Larson,[4] J. W. Bonnell,[4] O. Le Contel,[5] A. Roux,[5] and U. Auster[6]

Received 4 September 2009; revised 5 December 2009; accepted 30 December 2009; published 8 June 2010.

[1] A statistical survey of plasma densities and electron distributions (0.5–100 keV) is performed using data obtained from the Time History of Events and Macroscale Interactions During Substorms spacecraft in near-equatorial orbits from 1 July 2007 to 1 May 2009 in order to investigate optimum conditions for whistler mode chorus excitation. The plasma density calculated from the spacecraft potential, together with in situ magnetic field, is used to construct global maps of cyclotron and Landau resonant energies under quiet, moderate, and active geomagnetic conditions. Statistical results show that chorus intensity increases at higher *AE* index, with the strongest waves confined to regions where the ratio between the plasma frequency and gyrofrequency, f_{pe}/f_{ce}, is less than 5. On the nightside, large electron anisotropies and intense chorus emissions indicate remarkable consistency with the confinement to 8 R_E. Furthermore, as injected plasma sheet electrons drift from midnight through dawn toward the noon sector, their anisotropy increases and peaks on the dayside at $7 < L < 9$, which is well correlated with intense chorus emissions observed in the prenoon sector. These statistical results are generally consistent with the generation of both lower-band and upper-band chorus through cyclotron resonant interactions with suprathermal electrons (1–100 keV). Two typical events on the nightside and dayside are studied in greater detail and additional interesting features are identified. Pancake distributions of electrons with energy below ~2 keV, which could be responsible for the excitation of upper-band chorus, are observed at lower L shells (<7) on the nightside and at larger L shells (>6) on the dayside. In addition, very isotropic distributions at a few keV, which may be produced by Landau resonance and contribute to the formation of the typical gap in the chorus spectrum near 0.5 f_{ce}, are commonly observed on the dayside.

Citation: Li, W., et al. (2010), THEMIS analysis of observed equatorial electron distributions responsible for the chorus excitation, *J. Geophys. Res.*, *115*, A00F11, doi:10.1029/2009JA014845.

1. Introduction

[2] Chorus emissions are intense whistler mode waves, which are excited in the low-density region outside the plasmapause, in association with the injection of plasma sheet electrons into the inner magnetosphere. Chorus emissions typically occur in two frequency bands (banded chorus), the lower band ($0.1\ f_{ce} < f < 0.5\ f_{ce}$) and upper band ($0.5\ f_{ce} < f < 0.7\ f_{ce}$) with a gap at 0.5 f_{ce}, where f_{ce} is the equatorial electron cyclotron frequency [*Burtis and Helliwell*, 1969; *Tsurutani and Smith*, 1977; *Hayakawa et al.*, 1984; *Koons and Roeder*, 1990; *Sazhin and Hayakawa*, 1992; *Santolík et al.*, 2003; *Bell et al.*, 2009]. The source region of chorus waves is generally believed to be located outside the plasmapause near the geomagnetic equator [*LeDocq et al.*, 1998; *Lauben et al.*, 2002; *Parrot et al.*, 2003; *Santolík et al.*, 2003]. However, *Tsurutani and Smith* [1977] proposed that on the dayside chorus can also be generated at high magnetic latitudes (20°–50°) within "minimum B pockets" at relatively higher L shells. More recently, several studies [e.g., *Vaivads et al.*, 2007; *Tsurutani et al.*, 2009] reported observations of chorus waves with a possible source at high latitudes on the dayside. Chorus emissions are predominantly observed during geomagnetically disturbed conditions [*Tsurutani and Smith*, 1974; *Meredith et al.*, 2001, 2003; *Miyoshi et al.*, 2003] in association with enhanced fluxes of suprathermal electrons [*Anderson and Maeda*, 1977; *Meredith et al.*, 2002; *Miyoshi et al.*, 2007].

[1]Department of Atmospheric and Oceanic Sciences, University of California, Los Angeles, California, USA.
[2]Solar-Terrestrial Environment Laboratory, Nagoya University, Nagoya, Japan.
[3]Institute of Geophysics and Planetary Physics, Department of Earth and Space Sciences, University of California, Los Angeles, California, USA.
[4]Space Sciences Laboratory, University of California, Berkeley, California, USA.
[5]Laboratoire de Physique des Plasmas, Ecole Polytechnique, Université Pierre et Marie Curie, Paris 6, CNRS, Vélizy, France.
[6]Institut für Geophysik und extraterrestrische Physik, Technischen Universität Braunschweig, Braunschweig, Germany.

0148-0227/10/2009JA014845

[3] Observations from the OGO 5 satellite showed that equatorial chorus emissions are dominant at 0000–0900 MLT, while high-latitude chorus emissions are only found on the dayside with the maximal occurrence at 1200 MLT [*Burton and Holzer*, 1974; *Sazhin and Hayakawa*, 1992]. More recent studies [*Meredith et al.*, 2001; *Meredith et al.*, 2003; *Bortnik et al.*, 2007; *Li et al.*, 2009a] showed that nightside chorus waves are confined to the equatorial region at magnetic latitudes below 15°, while strong dayside chorus emissions can extend to latitudes above 30°. *Li et al.* [2009a] also found that the occurrence rate of dayside chorus is higher than that on the nightside and dayside chorus can extend to larger radial distances compared to the nightside chorus (which is confined within 8 R_E), consistent with *Tsurutani and Smith* [1977]. Although the excitation mechanism for upper-band chorus remains debatable [e.g., *Hashimoto and Kimura*, 1981; *Horne et al.*, 2003a], it has been generally accepted that lower-band chorus waves can be generated through a cyclotron resonance with anisotropic electrons with energies between a few and tens of keV [e.g., *Kennel and Petschek*, 1966; *Kennel and Thorne*, 1967; *Tsurutani and Smith*, 1974; *Nunn et al.*, 1997; *Chum et al.*, 2007; *Katoh and Omura*, 2007a, 2007b; *Omura et al.*, 2008]. Therefore evaluating electron distributions in this energy range should provide a better understanding of the generation and global distributions of chorus waves.

[4] An investigation of chorus wave normal angles was performed by several studies in the equatorial magnetosphere. *Goldstein and Tsurutani* [1984] and *Hayakawa et al.* [1984] have shown that the wave normal at lower frequencies ($f < 0.3\ f_{ce}$) tends to be field-aligned. Using OGO 5 data, *Burton and Holzer* [1974] reported that wave normal distributions for unducted chorus near the equator is symmetric around 0° and confined within a cone angle of 20°. However, analyses of wave normal angles for upper-band chorus have led to widely diverse results, ranging from essentially field-aligned [e.g., *Lauben et al.*, 2002] to highly oblique with wave normal angles close to the resonance cone [e.g., *Hayakawa et al.*, 1984; *Muto et al.*, 1987]. More recently, *Breneman et al.* [2009] reported that correlation regions close to the magnetic equator emit lower-band chorus with wave normal angles generally confined within 20°, while upper-band chorus is generally found at higher wave normal angles of between −20° and −40°, and at 50°. Despite above reported studies, general agreement on chorus wave normal distributions has not been reached, and this controversial topic remains for further investigation. However, because upper-band chorus emissions generally exhibit a strong fluctuating magnetic field component [e.g., *Tsurutani and Smith*, 1974; *Lauben et al.*, 1998], we assume that chorus waves are electromagnetic for the purpose of evaluating typical resonant electron energies. This is later confirmed in our case study analysis on the dayside.

[5] Electron distributions responsible for chorus generation have been studied previously, but comprehensive information on the resonant electron distributions responsible for chorus excitation has still not been extensively available yet. Very few spacecraft in the dominant regions of chorus generation have been equipped to observe both waves and particles. An extensive study by *Tsurutani et al.* [1979] using OGO 5 data showed that the correlation between chorus activity and energetic (>55 keV) electrons is more typical for equatorial chorus, while for dayside high-latitude chorus no such correlation was observed. Later, *Isenberg et al.* [1982] reported simultaneous observations of electrons in the range of 10–100 keV and chorus activities on the dawnside using SCATHA data and concluded that dawnside chorus is generated by substorm-injected, anisotropic electrons with energies between 10 and 100 keV. More recently, using CRRES data, statistical analyses by *Bortnik et al.* [2007] and *Meredith et al.* [2009] have also captured important characteristics of the global distribution of electron fluxes. Perpendicular electron fluxes (0.213–16.5 keV) observed by CRRES, categorized by various levels of magnetic activity, showed little dependence on MLT during quiet times ($AE < 100$ nT) but pronounced electron flux enhancements on the nightside and penetration toward lower L shells during disturbed times [*Bortnik et al.*, 2007] due to enhanced convection electric fields [e.g., *Korth et al.*, 1999]. Consequently, the global distribution of electron fluxes shows pronounced day-night asymmetry, with almost an order of magnitude drop in flux between midnight and noon. However, the data coverage of CRRES was limited for evaluating the global distribution of electrons which are responsible for chorus generation, since the CRRES orbit was confined to 7 R_E with a pronounced data gap in the prenoon equatorial sector at $L > 5$; a region where chorus waves are intense with a high occurrence rate [*Li et al.*, 2009a]. *Denton et al.* [2005] performed a statistical analysis using LANL data in the geosynchronous orbit and found that the anisotropy of hot electrons (30 eV–45 keV) on the dayside was generally larger than that on the nightside. More comprehensive information on the injected electron phase space density (PSD) and anisotropy over the entire inner magnetosphere is required to understand the global distribution of chorus excitation and its effect on energetic radiation belt electrons [*Meredith et al.*, 2001; *Summers et al.*, 2002; *Horne and Thorne*, 2003; *Horne et al.*, 2003b, 2005; *Meredith et al.*, 2003; *Albert*, 2005; *Li et al.*, 2007; *Thorne et al.*, 2007; *Li et al.*, 2009a].

[6] The main objective of this study is to present statistical results of the global distribution of electron pitch angle distributions (PADs) near the equator between 5 and 10 R_E, in the region which has not been completely covered by previous spacecraft, in order to further identify the mechanism for the chorus wave excitation. In section 2, we briefly describe the data available from the Time History of Events and Macroscale Interactions During Substorms (THEMIS) spacecraft. Statistical results of plasma densities and minimum resonant energies are presented in section 3 to evaluate electron energies responsible for potential chorus excitation and damping. In section 4, we show global distributions of the electron PSD and anisotropy for various levels of magnetic activity. Two typical chorus events are discussed in section 5 in order to identify interesting features of the electron distributions responsible for the wave excitation on the nightside and dayside in greater detail. In section 6 we summarize and discuss the principal results of the present study.

2. THEMIS Data

[7] The THEMIS spacecraft, comprising five probes in near-equatorial orbits with apogees above 10 R_E and peri-

gees below 2 R_E [*Angelopoulos*, 2008], are ideally situated to measure chorus emissions and corresponding electron distributions in the equatorial magnetosphere. Electron PAD data for lower energies (a few eV up to 30 keV) are collected by the Electro-Static Analyzer (ESA) [*McFadden et al.*, 2008], and the Solid State Telescope (SST) can measure electron PADs from 25 keV to 1 MeV [*Angelopoulos*, 2008]. The Fluxgate Magnetometer (FGM) [*Auster et al.*, 2008] measures background magnetic fields and their low-frequency fluctuations (up to 64 Hz) in the near-Earth space. FGM data in this study are utilized to evaluate local electron cyclotron frequencies in order to scale chorus frequencies. The Search-Coil Magnetometer (SCM) [*Roux et al.*, 2008; *Le Contel et al.*, 2008] measures low-frequency magnetic field fluctuations and waves in three orthogonal directions over a frequency range from 0.1 Hz to 4 kHz. The Electric Field Instrument (EFI) provides waveforms and three-axis spectral measurements of ambient electric fields from DC up to 8 kHz. Individual sensor potentials are also measured, providing on-board and ground-based calculation of spacecraft floating potentials and high-resolution plasma density measurements [*Bonnell et al.*, 2008]. The total electron density is inferred from the spacecraft potential and electron thermal speed measured by the EFI and ESA instruments, respectively, including the cold plasma population in addition to the hot plasma component measured by ESA. The electron density outside the plasmapause is calibrated by a statistical comparison with 1-year (2008) ESA observations for each spacecraft, while the plasmasphere density is estimated by fitting the statistical density profile given by *Sheeley et al.* [2001]. Details of the method are described by *Mozer* [1973] and *Pedersen et al.* [1998], and the obtained electron densities are associated with an uncertainty generally within a factor of ~2. The SCM and EFI output waveforms are digitized and processed by the Digital Fields Board (DFB) [*Cully et al.*, 2008]. The resulting amplitude of the electric field parallel to the longer pair of antenna in the spin plane and the magnetic field perpendicular to the electric field in the spin plane is filtered through multiple passbands (filter bank data). Subsequently, it is included in the survey mode telemetry, covering most orbits with a measurement cadence of 4 s in six logarithmically spaced frequency bands in a range of ~2 Hz–4 kHz. Both search coil and electric field telemetry include waveforms and FFT processed data. For particle burst data, the wave spectral density is obtained with a higher frequency resolution (up to 64 bands). Equipped with the high-quality electric field instrument (EFI), magnetic field instrument (SCM), and particle instruments (ESA and SST), the THEMIS spacecraft offer an excellent opportunity to study characteristics of whistler mode waves and corresponding electron distributions in the dominant chorus source region.

3. Statistical Analysis of the Plasma Density and the Electron Resonant Energy

3.1. Global Distributions of the Plasma Density

[8] The plasma density plays an important role in controlling chorus generation, since it affects the minimum electron resonant energy for a given wave frequency. Since chorus waves are generated outside the plasmapause, equation (1) [*Moldwin et al.*, 1994; *Sheeley et al.*, 2001] is used to distinguish between plasmaspheric and trough-like densities

$$n_b = 10 \times \left(\frac{6.6}{L}\right)^4. \quad (1)$$

Plasma densities at or above n_b for a given L shell are considered to be plasmaspheric and are excluded from this study, while values below n_b are considered to be trough-like. Figure 1a shows the global distribution of the trough-like plasma density observed between 5 and 10 R_E at all MLTs categorized by different levels of magnetic activity. Plasma density data obtained in the chorus source region at latitudes smaller than 10° are first mapped to the magnetic equator using a dipole magnetic field model (with an uncertainty of $\Delta L < 0.3$, compared to Tsyganenko 96 magnetic field model [*Tsyganenko and Stern*, 1996]). Then the density data are binned as a function of L in steps of 0.2 L and MLT with an interval of 1 h, and the value in each bin represents the mean density. Generally, the plasma density on the dayside is larger than that on the nightside, peaking in the postnoon sector due to the presence of plumes. Even though the density data in each bin tend to only include trough-like density, it is possible to observe the effects of plasmasphere erosion and plume formation with the increasing *AE*. It is also interesting to note that during geomagnetically active times ($AE > 300$ nT), the plasma density on the nightside at L shells between 6 and 8 is larger than that during quiet times, which is probably due to the injection of plasma sheet electrons. The plasma density in the geosynchronous orbit is about 2 cm^{-3} at midnight, ~3 cm^{-3} at noon, and peaks around 1800 MLT with ~5 cm^{-3}, roughly consistent with the result of *Sheeley et al.* [2001].

[9] Figure 1b shows the global distribution of the ratio (mean value) of the plasma frequency to the electron cyclotron frequency (f_{pe}/f_{ce}), which is also mapped to the equator using data measured at latitudes less than 10°. Electron cyclotron frequencies are calculated from in situ magnetic field data measured by the FGM instrument. Interestingly, although the plasma density increases from midnight through dawn to the noon sector, the ratio, f_{pe}/f_{ce} decreases, particularly at $L > 7$, due to the dominant effect of increasing electron cyclotron frequencies caused by the magnetospheric compression on the dayside [e.g., *Li et al.*, 2009a]. On the nightside, f_{pe}/f_{ce} is higher at larger L shells mainly due to the weaker background magnetic field, while in the prenoon sector the ratio is roughly independent of L. It is interesting to note that the most intense chorus waves (Figure 1c) are observed in regions where the ratio f_{pe}/f_{ce} is smaller than ~5, i.e., at $L < 7$ on the nightside and at relatively higher L shells (>7) in the prenoon sector. Here we need to mention that the absolute number of 5 is an approximate value, since density values obtained from the THEMIS data contain uncertainties (generally within a factor of ~2). *Santolik et al.* [2005] performed a statistical survey using Double Star TC-1 spacecraft to investigate dawn chorus (mainly from 0600 MLT to 1200 MLT) and showed that chorus intensity increases at L shells above 6, with an extension of lower-band chorus up to L of 11–12. These regions associated with strong chorus from the dawn

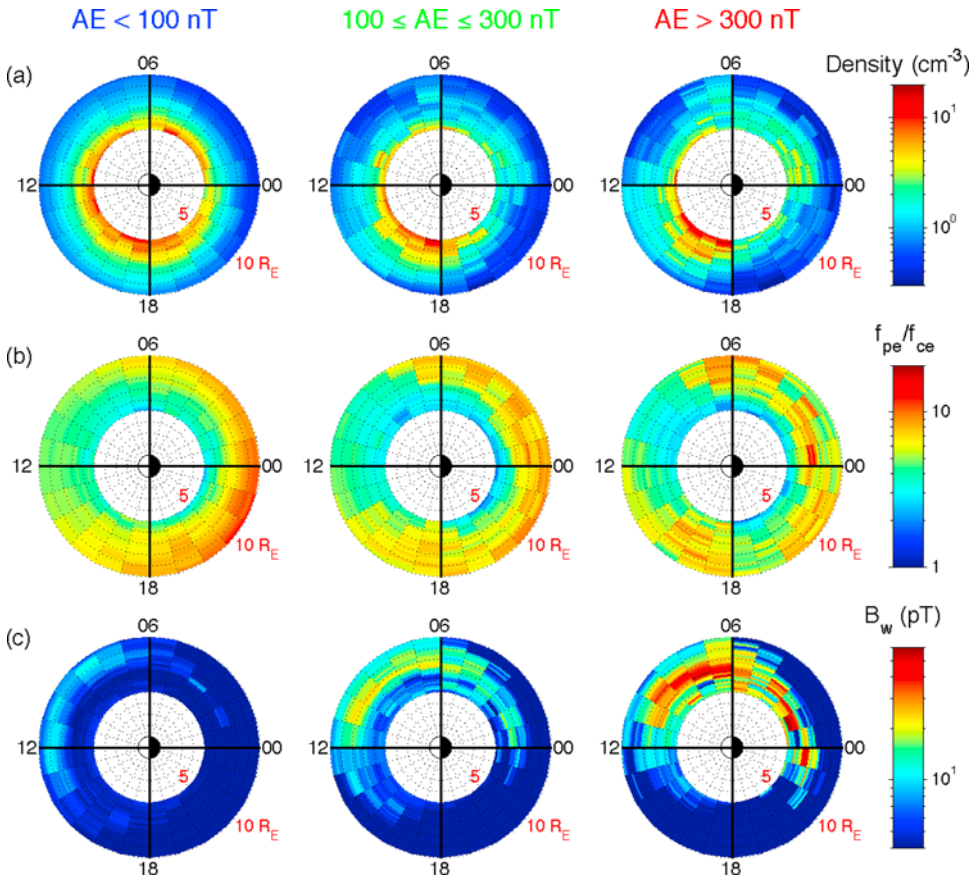

Figure 1. Global distributions of (a) mean plasma density (cm^{-3}), (b) mean value of the ratio of plasma frequency to the local electron cyclotron frequency, and (c) RMS wave amplitude (pT) at different levels of the *AE* index. All data are for the equatorial distribution at magnetic latitudes less than 10° and shown in regions between 5 and 10 R_E at all MLTs.

to the noon sector are consistent with regions containing low f_{pe}/f_{ce}, generally less than 5.

3.2. Global Distributions of the Minimum Resonant Energy

[10] Electrons undergo adiabatic gyro, bounce, and drift motion in the radiation belts. The first adiabatic invariant of the electron motion can be violated through resonant interactions with plasma waves whose frequencies ($\omega = 2\pi f$) are Doppler-shifted to a multiple (n = 0, ±1, ±2, …) of the relativistic electron gyrofrequency. This resonance condition is expressed as

$$\omega - k_{//} v_{//} = n|\Omega_e|/\gamma, \tag{2}$$

where $\gamma = [1 - (v/c)^2]^{-1/2}$ is the relativistic factor, v is the electron velocity, c is the speed of light, $|\Omega_e| = 2\pi f_{ce}$, and $k_{//}$ and $v_{//}$ are components of the wave propagation vector and particle velocity along the ambient magnetic field [e.g., *Thorne et al.*, 2005].

[11] First-order cyclotron (n = 1) and Landau (n = 0) resonant interactions mainly control growth and damping rates of whistler mode waves [*Kennel and Petschek*, 1966; *Kennel and Thorne*, 1967]. For chorus waves with frequencies of $\omega_{LH} \ll \omega < \Omega_e$ (ω_{LH} is the lower hybrid frequency) and propagating with a wave normal angle of θ, the well-known quasi-longitudinal whistler dispersion relation [*Stix*, 1962] is

$$n^2 \cong \frac{\omega_{pe}^2}{\omega\Omega_e} \frac{1}{(\cos\theta - \omega/\Omega_e)}, \tag{3}$$

where n is the refractive index and ω_{pe} is the plasma frequency. Consequently, the minimum energy for nonrelativistic electrons which undergo the first-order cyclotron resonance with parallel propagating chorus can be expressed as

$$E_{\min}^{\text{Cyclotron}} = \frac{m_e c^2}{2} \frac{\Omega_e^2}{\omega_{pe}^2} \frac{\Omega_e}{\omega} \left(1 - \frac{\omega}{\Omega_e}\right)^3, \tag{4}$$

where m_e is the electron mass.

[12] Similarly, the minimum energy for electrons which experience Landau resonance through oblique chorus waves with a wave normal angle of θ is obtained as

$$E_{\min}^{\text{Landau}} = \frac{m_e c^2}{2} \frac{\Omega_e^2}{\omega_{pe}^2} \frac{\omega}{\Omega_e} \left(\frac{\cos\theta - \omega/\Omega_e}{\cos^2\theta}\right). \tag{5}$$

The statistical results in Figure 1b are used to calculate the minimum resonant energies for the first-order cyclotron and

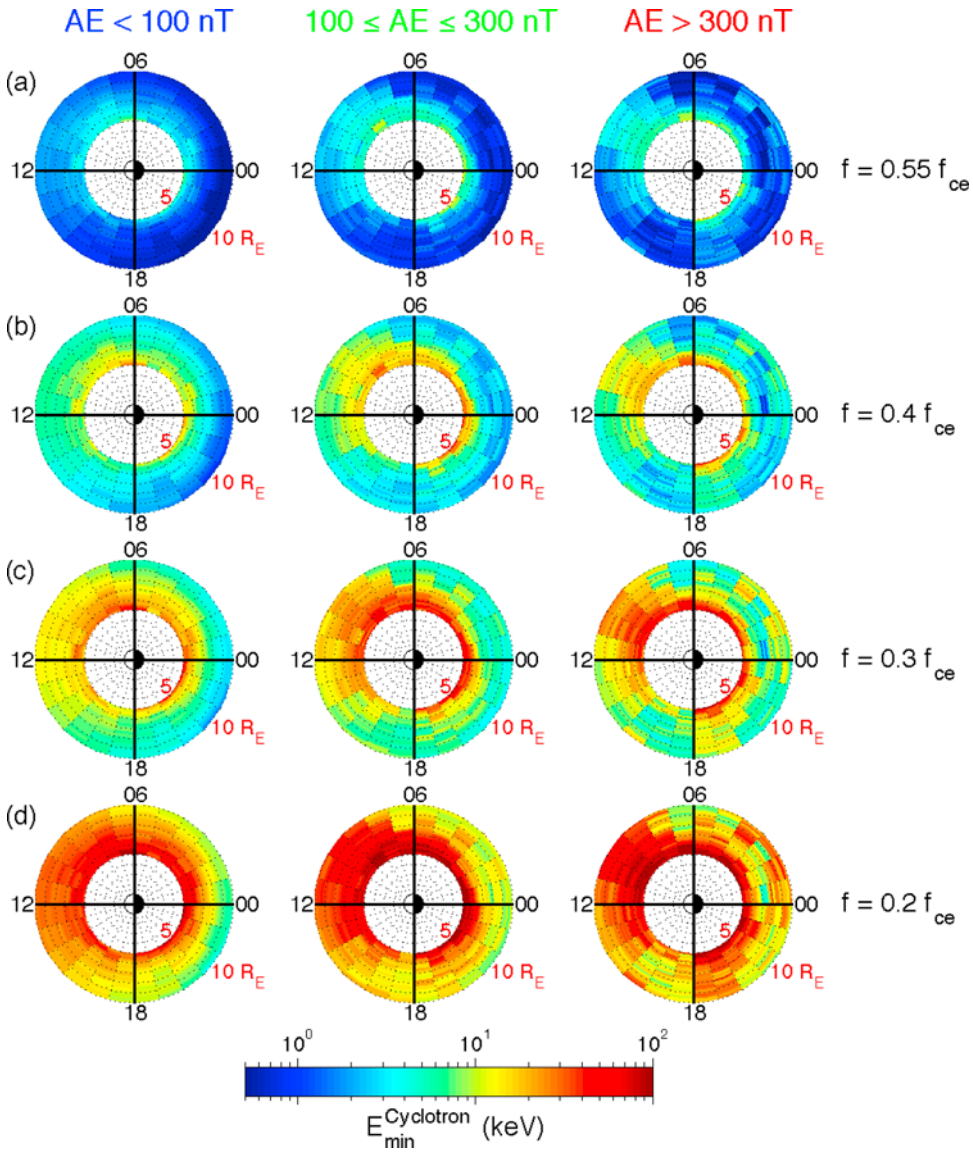

Figure 2. Global distributions of the mean electron minimum energy (keV) for the cyclotron resonance with parallel propagating chorus waves with different frequencies ((a) 0.55 f_{ce}, (b) 0.4 f_{ce}, (c) 0.3 f_{ce}, and (d) 0.2 f_{ce})). Left, middle, and right columns indicate minimum resonant energy at different levels of the *AE* index.

Landau resonance through equations (4) and (5). Upper-band chorus tends to have a peak intensity near 0.55 f_{ce}, while lower-band chorus peaks at 0.3–0.4 f_{ce} on the nightside and at 0.2–0.3 f_{ce} on the dayside [e.g., *Bortnik et al.*, 2007; *Shprits et al.*, 2007]. Figure 2 shows statistical results of the minimum energy (mean value) for the first-order cyclotron resonance at different frequencies during various levels of magnetic activity. Figure 2a is for the upper-band chorus with a frequency of 0.55 f_{ce} and Figures 2b, 2c, and 2d are for the lower-band chorus with frequencies of 0.4 f_{ce}, 0.3 f_{ce}, and 0.2 f_{ce}. At each frequency, the minimum cyclotron resonant energy tends to be larger over a broad range of L shells in the prenoon sector and at low L shells ($L < 6$) on the nightside. In addition, the minimum resonant energy exhibits a slight increase at higher *AE*. Electrons resonating with upper-band chorus contain small resonant energies between 500 eV and a few keV. For lower-band chorus, minimum resonant energies are considerably larger (>10 keV) and increase with decreasing wave frequencies (see equation (4)). It is important to note that for typical nightside chorus waves with amplitudes peaking around 0.3 f_{ce}, the minimum resonant energies are generally less than ~30 keV, while for the typical dayside chorus peaking around 0.2 f_{ce}, the minimum resonant energy could be as high as 100 keV.

[13] Similarly, Figure 3 shows the global distribution of the minimum electron energy of the Landau resonance for various wave frequencies obtained by using equation (5) categorized by the *AE* index. Here we assume that waves are propagating with a wave normal angle of 30°, where the Landau resonance starts to dominate [*Kennel*, 1966; *Kennel and Thorne*, 1967]. For the entire range of chorus emis-

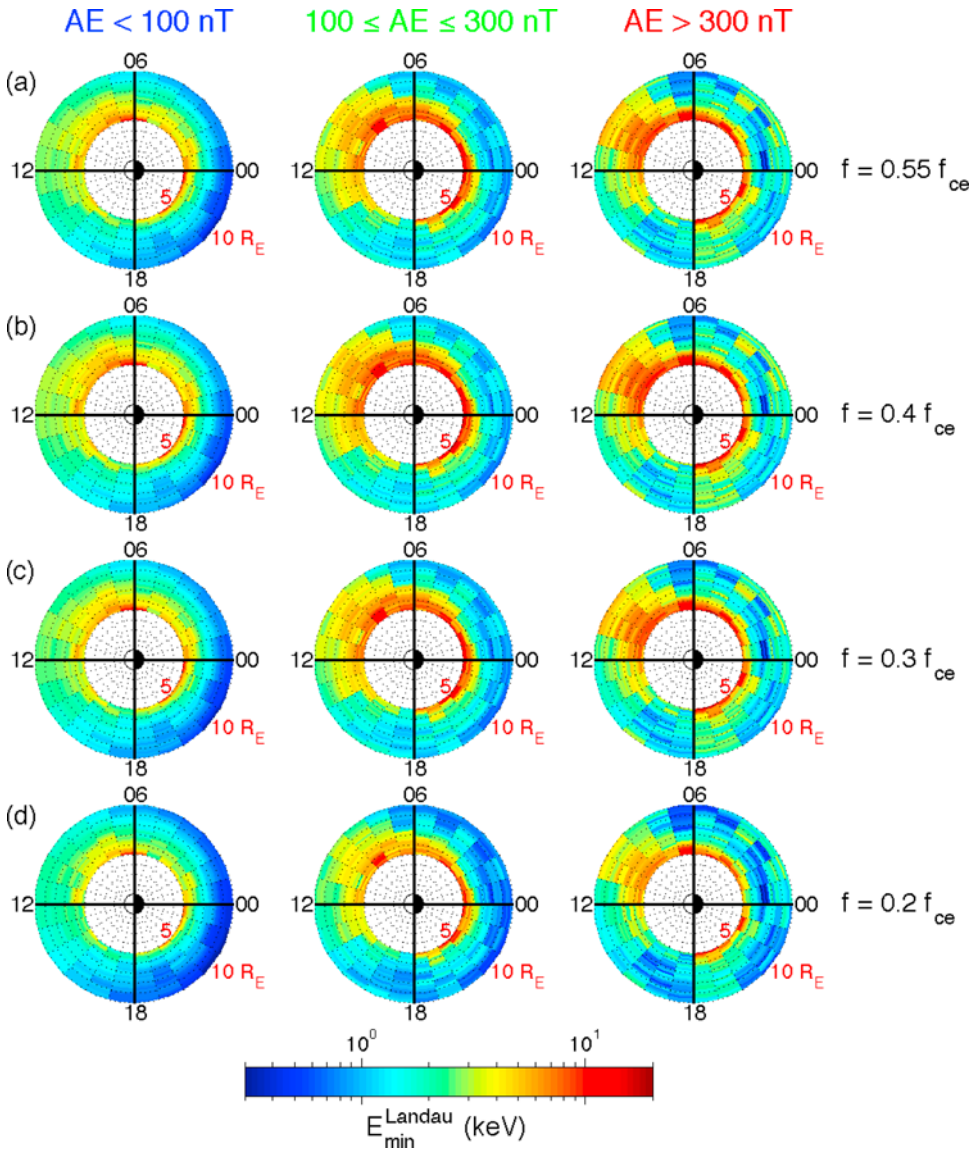

Figure 3. The same format as Figure 2 but for the mean electron minimum energy (keV) for the Landau resonance when chorus waves propagate with a wave normal angle of 30°.

sions, the minimum Landau resonant energy exhibits little dependence on wave frequency and generally lies in a range of a few keV in spatial regions where chorus is most intense (Figure 1c). These computed minimum resonant energies will be used in section 4 as a proxy to evaluate the corresponding electron distributions responsible for the chorus excitation.

4. Statistical Analysis of the Electron Phase Space Density and the Pitch Angle Anisotropy

[14] The theory of particle drift motions in a distorted magnetosphere has been reviewed by *Roederer* [1967] and *Roederer and Schulz* [1969]. Conservation of the first adiabatic invariant requires that equatorially mirroring particles move along contours of constant equatorial magnetic field. On the other hand, particles mirroring far from the equator tend to drift so as to keep the length of their bounce paths about the same while preserving the value of the magnetic field at their mirror points. Consequently, in a distorted terrestrial magnetic field, particles originating near midnight with pitch angles near 90° move to a larger radial distance, as they are transported toward the dayside, while particles with pitch angles near the loss cone remain at roughly the same radial distance to the Earth [e.g., *Sibeck et al.*, 1987]. Owing to the magnetopause shadowing, a pronounced reduction in particle fluxes near 90° pitch angles is generally observed on the nightside for high-energy electrons for which the magnetic drift is dominant. Such "butterfly distributions," originating due to the effects of drift shell splitting, are usually apparent outside 6 R_E throughout the nightside [*West et al.*, 1973; *Sibeck et al.*, 1987]. In the inner magnetosphere, particle PADs tend to peak at 90° and fall off smoothly toward smaller pitch angles. Such PADs with positive anisotropies, resulting from the particle pitch angle diffusion and the loss of particles with low pitch

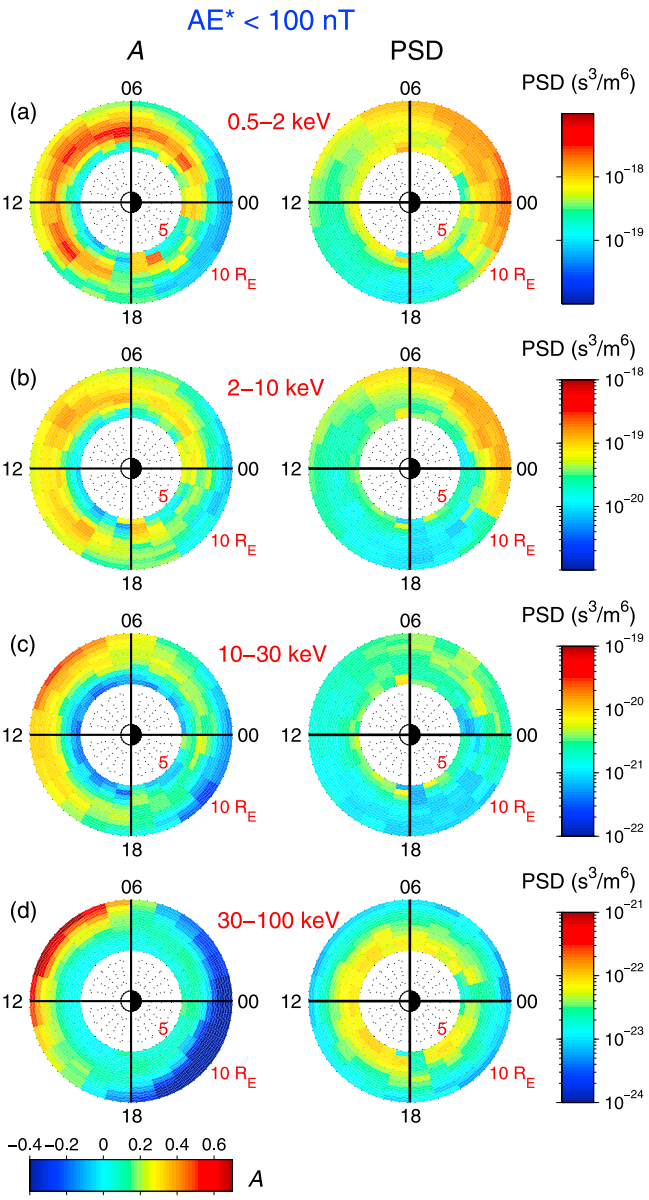

Figure 4. Global distributions of the averaged electron anisotropy and omni-directional electron PSD (s^3/m^6) during quiet times when $AE^* < 100$ nT for electrons with different energies ((a) 0.5–2 keV, (b) 2–10 keV, (c) 10–30 keV, (d) 30–100 keV)).

angles by precipitation into the atmosphere, tend to be formed throughout the dayside magnetosphere, as well as on the nightside within 6 R_E of the Earth [*Sibeck et al.*, 1987].

[15] Highly anisotropic electron PADs narrowly peaking near 90°, are called pancake PADs based on their appearance in velocity space [*Meredith et al.*, 1999]. These pancake PADs are only observed near the magnetic equator because electrons with pitch angles in a range between 70° and 110° mirror within ±10° of the magnetic latitude. Several reasons have been proposed to explain pancake PADs. *Lyons et al.* [1972] described how whistler mode wave-particle interaction could result in pancake electron PADs. *Meredith et al.* [1999] showed that pancake distributions develop from freshly injected distributions on a timescale greater than 2 h. This newly injected population is frequently associated with strong electrostatic electron cyclotron harmonic (ECH) waves and whistler mode waves. The pancake distributions are therefore likely to be caused by a combination of whistler mode and ECH wave activities. *Meredith et al.* [1999] suggest that whistler mode waves play a dominant role in the formation of pancake distributions outside $L = 6.0$, whereas inside $L = 6.0$ and, in particular, in the vicinity of the plasmapause, ECH waves also play a significant role.

[16] In this study, THEMIS ESA and SST data are used to provide a global picture of equatorial (|MLAT| < 10°) electron PADs in the chorus source region between 5 and 10 R_E. Figures 4, 5, and 6 show statistical analyses of the

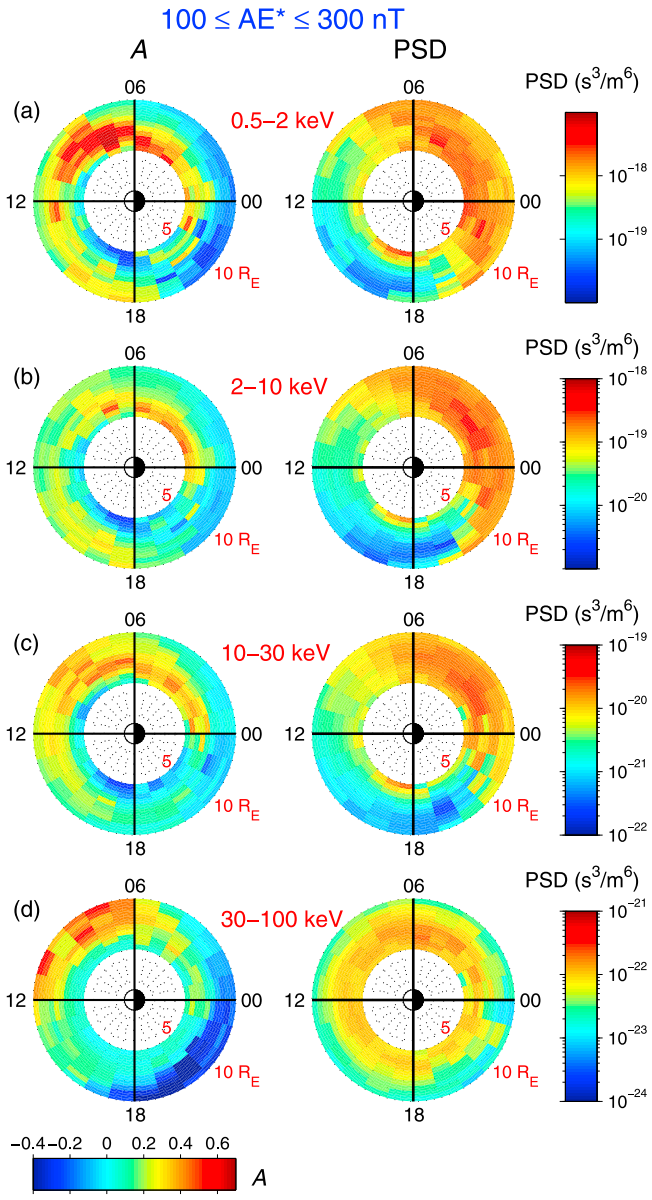

Figure 5. The same as Figure 4 but when $100 \leq AE^* \leq 300$ nT.

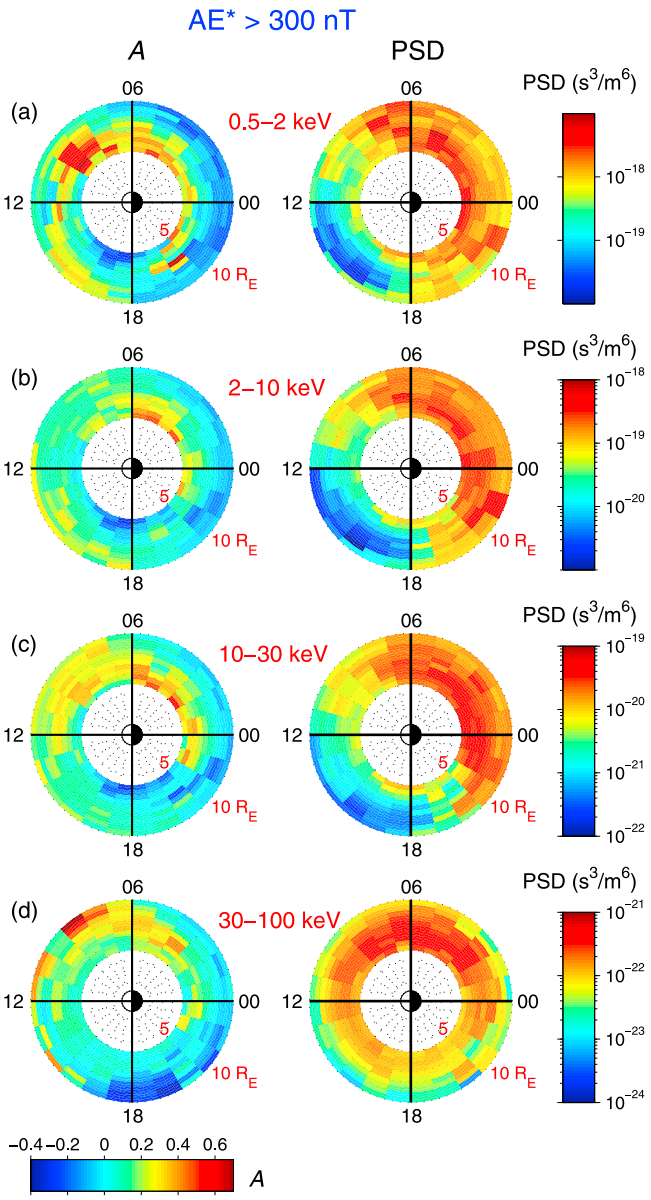

Figure 6. The same as Figure 4 but when $AE^* > 300$ nT.

global distribution of the averaged electron anisotropy (left column) and omnidirectional electron PSDs (right column) at appropriate energies responsible for the chorus generation (a: 0.5–2 keV; b: 2–10 keV; c: 10–30 keV; d: 30–100 keV) during quiet ($AE^* < 100$ nT), moderately active ($100 \leq AE^* \leq 300$ nT), and highly disturbed ($AE^* > 300$ nT) conditions. Here AE^* is the mean value of the AE index during the previous 1 h. In Figures 4, 5, and 6, top panels are presumably corresponding to electron energies responsible for the upper-band chorus, and bottom three panels are mainly for the lower-band chorus. The electron distribution data are obtained at magnetic latitudes less than 10° with a bin size of 0.5 L × 1 MLT, and the value in each bin represents the mean value. Here electron PSD is calculated from the averaged electron energy flux in the specified energy range and electron anisotropy is calculated for a fixed electron kinetic energy (mean value in the specified energy range) [e.g., *Chen et al.*, 1999] as follows:

$$A = \frac{\int_0^{\pi/2} f(E,\alpha_0)\sin^3\alpha_0 d\alpha_0}{2\int_0^{\pi/2} f(E,\alpha_0)\cos^2\alpha_0 \sin\alpha_0 d\alpha_0} - 1, \quad (6)$$

where α_0 is the equatorial pitch angle, E is the kinetic energy, and f is the electron PSD. $A = 0$ corresponds to pitch angle isotropy, $A > 0$ represents PADs peaking at 90°, while $A < 0$ indicates a PSD minimum at 90°.

[17] Under quiet conditions (Figure 4), the electron PSD remains relatively small at all locations, and there is a modest decrease in PSD at energies less than 10 keV along expected drift trajectories from the nightside toward the dayside. Preferential loss of electrons with lower pitch angles by precipitation into the atmosphere is probably responsible for the observed increase in electron anisotropy on the dayside. At higher energies (>10 keV), where the magnetic gradient drift becomes important, there is a much more pronounced increase in pitch angle anisotropy on the dayside at $L > 7$, due to drift shell splitting. At even higher energies shown in Figure 4d (30–100 keV) electron PSDs show little MLT dependence, and electron PADs at $L > 7$ evolve from negative anisotropy at night to strongly positive A on the dayside due to drift shell splitting.

[18] Under moderately active conditions (Figure 5) and extremely disturbed times (Figure 6), the electron PSD on the nightside increases dramatically compared to that at the quiet times due to the enhanced electron injection from the plasma sheet. Interestingly, the PSD at noon remains comparable to that during quiet conditions, leading to a much stronger day-night asymmetry of the global distribution of the electron flux particularly for the lower-energy electrons (<30 keV). For electrons with energies of 1–30 keV, which mainly contribute to the nightside chorus generation, anisotropy becomes larger on the nightside at $L < 8$ during higher geomagnetic activity and thus provide a source of free energy for the cyclotron resonant generation of the strong chorus emissions confined within ~8 R_E (Figure 1c). On the dayside, where the typical cyclotron resonant energy of lower-band chorus is 10–100 keV (Figure 2), resonant electron anisotropy is strongly enhanced in the prenoon sector at $L > 7$ (Figures 5c, 5d, 6c, and 6d), again consistent with the spatial region of most intense chorus emissions (Figure 1c). Furthermore, on the dayside, the decrease in electron PSD is less pronounced for higher-energy electrons (Figures 5d and 6d). Interestingly, for 30–100 keV electrons located in the prenoon sector, anisotropy builds up at 6.5–10 R_E, while a substantial increase in PSD compared to that at quiet time (Figure 4d) is identified at 5–9 R_E. The combination of the above two facts could produce strong lower-band chorus waves in the prenoon sector peaking around 8 R_E, consistent with the chorus distribution shown in Figure 1c.

[19] Under geomagnetically active conditions, when intense waves are present, the omnidirectional electron PSD decreases dramatically from midnight through dawn to noon for low-energy electrons (0.5–10 keV) presumably due to pitch angle scattering close to the strong diffusion limit by chorus waves [e.g., *Ni et al.*, 2008; *Su et al.*, 2009]. For these low-energy electrons (0.5–10 keV), the convective

drift time is several hours [*Chen and Schulz*, 2001a, 2001b], which is considerably larger than the timescale (<1 h) of strong diffusion [e.g., *Summers and Thorne*, 2003]. Consequently, the electron PSD decreases substantially during the drift from midnight through dawn to noon. In addition, dominance of the electric drift for low-energy electrons prevents them from drifting across the noon meridian, and most of them are transported toward the dayside magnetopause where these particles are ultimately lost. At higher energies (>10 keV), the magnetic gradient drift dominates, allowing injected electrons to be transported closer to the noon sector. At even higher energies (30–100 keV), it is important to note that the electron PSD becomes essentially independent of MLT. For these electrons, the gradient drift time from midnight to noon is less than 1 h, which is shorter than the typical timescale of scattering by waves [*Ni et al.*, 2008]. Loss to the atmosphere is therefore slower than magnetic drift for these high-energy electrons, facilitating them to drift around the entire dayside. Such high-energy electrons are also subject to drift shell splitting, which leads to the large anisotropy in the prenoon sector.

[20] During active geomagnetic conditions, electron anisotropy generally increases from midnight through dawn to the noon sector except for a limited energy range near a few keV, which show small positive anisotropies (Figure 6b) especially in the prenoon sector. This characteristic feature is clearly shown and further discussed in the event study on the dayside in the next section. Interestingly, such electrons could undergo Landau resonance with the excited chorus emissions, as we discussed in section 3, suggesting that Landau resonance could be the cause of the weak anisotropies.

5. Event Studies on the Nightside and Dayside

[21] In order to support the above statistical analysis of the global distribution of electron PADs responsible for chorus generation and to provide more information on the wave excitation process, two typical chorus events observed on the nightside and dayside are analyzed in detail below.

5.1. Nightside Event

[22] Figure 7 shows the time evolution of the *AE* index (Figure 7a), omnidirectional electron energy flux (Figure 7b), and anisotropy (Figure 7c) observed on 6 December 2008 by THEMIS D in the postmidnight sector, together with filter bank data of wave electric fields (Figure 7d) and magnetic fields (Figure 7e) recorded by EFI and SCM. The three white lines represent equatorial f_{ce}, 0.5 f_{ce}, and 0.1 f_{ce}. The plasma density inferred from the spacecraft potential and minimum resonant energy of cyclotron resonance for various wave frequencies are shown in Figures 7f and 7g, respectively. After ~0315 UT, a pronounced enhancement in electron energy flux occurs for energies between ~1 keV and a few tens of keV due to an injection from the plasma sheet, associated with the increase in *AE*. At energies larger than 5 keV, the injected electrons exhibit high anisotropy. Simultaneously, intense chorus waves are observed in both electric and magnetic instruments. The freshly injected electrons are initially highly anisotropic ($A > 1$), but the anisotropy is gradually reduced presumably due to quasi-linear relaxation during resonant interactions with the excited waves. As the electron fluxes are reduced and electron PADs become more isotropic after 0440 UT, chorus wave amplitudes also diminish. Six snapshots (indicated by black vertical arrows) of the ESA data have been selected to show the detailed electron PADs for various energies (Figure 7h). These particular six snapshots are chosen in order to show the clear variation in both wave amplitude and electron pitch angle distribution and include particular cases where particle burst data are available. We select 18 energy channels on a logarithmic scale between 100 eV and 200 keV, which are potentially important in the generation of chorus waves. At 0301:50 UT, low-energy electrons (<2 keV) exhibit pronounced pancake distributions, while high-energy electrons (>20 keV) responsible for chorus generation are relatively isotropic, which results in weak chorus waves. At 0317:60 UT, there is a clear injection of electrons with energy >10 keV, associated with the intensification of chorus waves. Between 0324 and 0344 UT (see the red arrow), particle burst data are available to provide a high time resolution on fluctuating electric and magnetic fields shown in Figures 8a and 8b. Both lower-band and upper-band chorus are clearly observed at 0327:42 UT, when the minimum resonance energy for the cyclotron resonance with the lower-band chorus (0.2–0.4 f_{ce}) is 3–20 keV and ~1 keV for the upper-band chorus (0.55 f_{ce}), as shown in Figure 7g. The anisotropic distribution ($A > 0$) of ~1 keV electrons may be responsible for the generation of upper-band chorus, while the anisotropic distribution ($A > 0$) of electrons with energies from a few to 25 keV is able to produce the strong lower-band chorus. Interestingly, a very isotropic distribution is found around a few keV, comparable to the Landau resonant energy and might be directly associated with the wave intensity minimum around 0.5 f_{ce} (Figure 8). At 0340:38 UT, when the distribution of ~1 keV electrons becomes more isotropized, upper-band chorus disappears correspondingly, while lower-band chorus is still present in association with the anisotropic distribution ($A > 0$) of 5–25 keV electrons. This result is consistent with the earlier finding of *Santolik et al.* [2005], who demonstrated that upper-band chorus is confined closer to the Earth, while lower-band chorus can extend to larger *L* shells. As the electron PSD decreases and becomes more isotropic at 0522:44 UT with the lower *AE*, chorus waves become weaker.

5.2. Dayside Event

[23] Figure 9 shows a dayside event observed by THEMIS A on 26 July 2008 in the same format as Figure 7. Compared to the nightside event, the dayside electron flux is much lower particularly for lower-energy electrons (<30 keV), and the amplitudes of chorus waves are correspondingly weaker, in association with the lower *AE* (Figure 9a). The intensification of chorus waves between 1340 and 1600 UT is associated with an increase in anisotropy for electrons with energies of 10–100 keV at $L \geq 8$. Interestingly, pronounced pancake distributions with very high anisotropy for low-energy electrons (0.1–2 keV) are commonly observed at *L* shells larger than 6, consistent with the statistical results shown in Figures 5a and 6a. Such distributions, which could lead to the excitation of upper-band chorus, can be produced during convective transport toward the dayside by the preferential scattering loss of

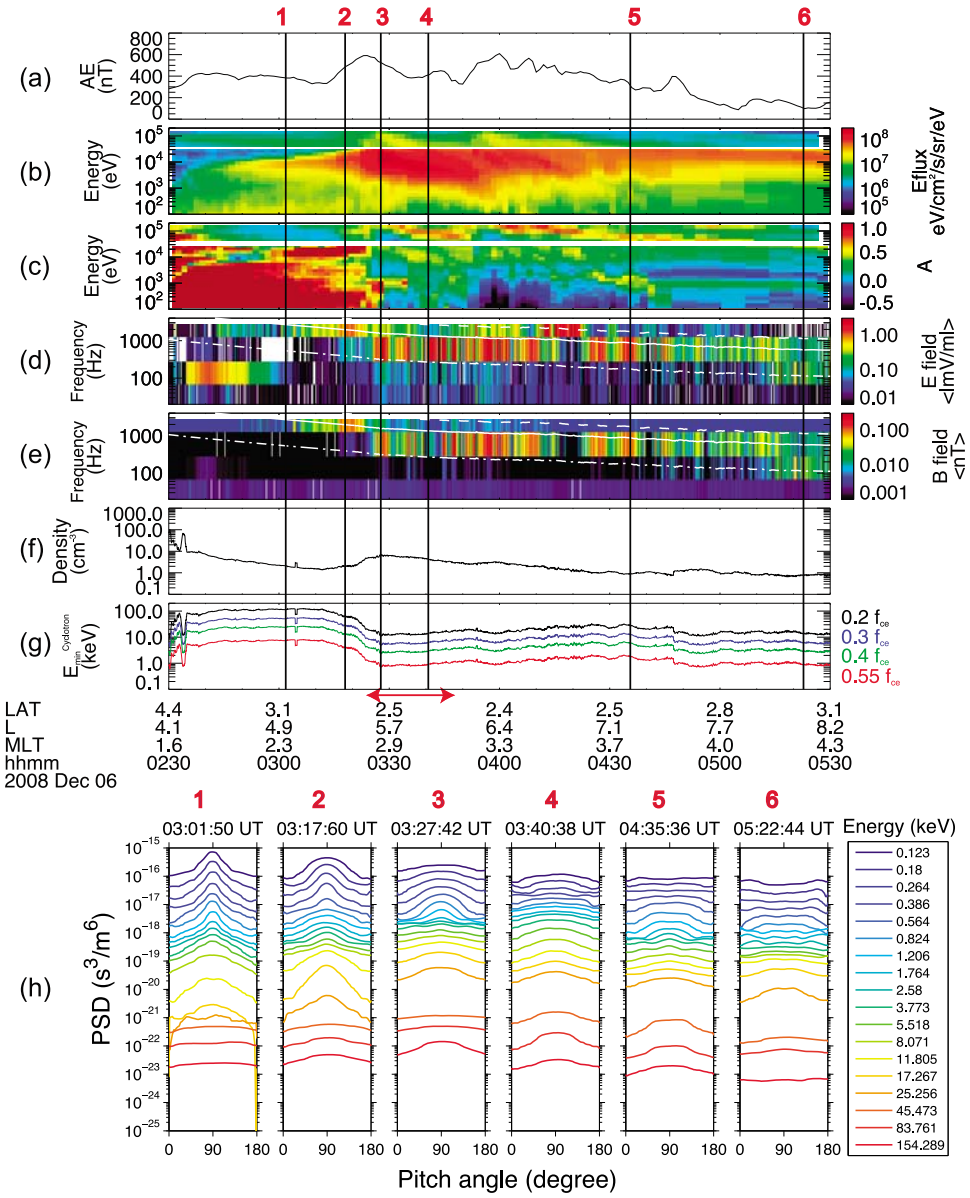

Figure 7. (a) *AE* index and ((b) and (c)) the time evolution of the omnidirectional electron energy flux (eV/cm^2/s/sr/eV) and anisotropy for various energies (100 eV–200 keV) from 0230 to 0530 UT on 6 December 2008 observed by Time History of Events and Macroscale Interactions During Substorms (THEMIS) D. (d) and (e) Amplitudes of wave electric and magnetic fields from the filter bank data given in units of mV/m and nT, respectively. The three white lines represent the equatorial electron cyclotron frequency (f_{ce}) (dashed), 0.5 f_{ce} (solid), and 0.1 f_{ce} (dash-dotted). (f) Total plasma density (cm^{-3}) inferred from the spacecraft potential. (g) Minimum electron energy for cyclotron resonance with chorus waves of various frequencies (black: 0.2 f_{ce}, blue: 0.3 f_{ce}, green: 0.4 f_{ce}, and red: 0.55 f_{ce}). The horizontal red arrow indicates the time period when particle burst data are available. (h) Six vertical black arrows represent six snapshots, which show the time evolution of the electron PSD as a function of the pitch angle for 18 different energy levels (0.123–154.289 keV).

electrons at low pitch angles during resonant interactions with chorus waves [*Ni et al.*, 2008; *Su et al.*, 2009]. Furthermore, owing to drift shell splitting, anisotropic distributions ($A > 0$) are expected to form at higher energies (>10 keV) in the prenoon sector (Figures 4c, 4d, 5c, and 5d). Interestingly, there is clear evidence of a very isotropic PAD (weak anisotropy shown in Figure 9c) for electrons of 1–5 keV. These isotropic distributions are more clearly shown in Figure 9h and could be related to Landau resonance, occurring in the same energy range.

[24] Here we also select six snapshots (indicated by black vertical arrows) to show electron PADs in more detail (Figure 9h). Inside the plasmasphere at 1237:26 UT, resonant electrons (>0.5 keV) exhibit very isotropic distribu-

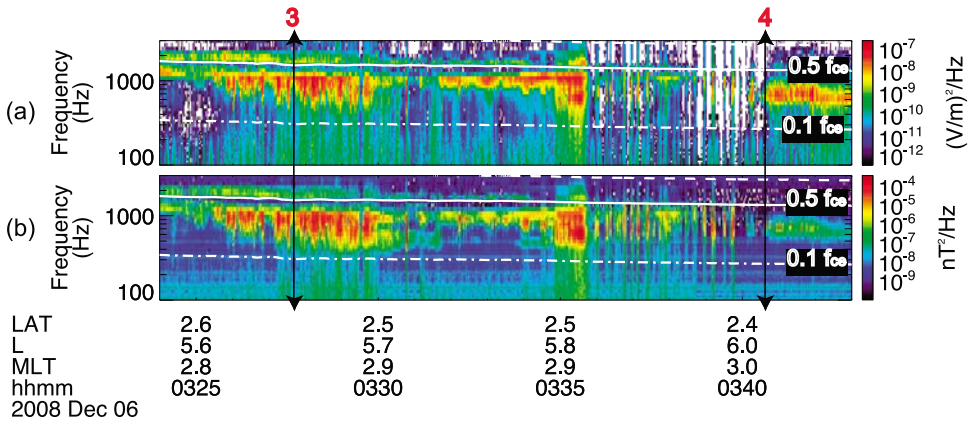

Figure 8. Spectrograms of (a) wave electric field and (b) magnetic field power spectral densities measured by EFI and SCM (particle burst mode available in the nightside event shown in Figure 7) in units of $V^2m^{-2}Hz^{-1}$ and nT^2Hz^{-1}. Three white lines indicate equatorial f_{ce} (dashed), 0.5 f_{ce} (solid), and 0.1 f_{ce} (dash-dotted). The black arrows represent the corresponding times when electron distribution data are shown in Figure 7g.

tions, and no chorus waves are observed simultaneously. At 1317:28 UT just outside the plasmapause, lower-band chorus is very weak due to the low anisotropy of cyclotron resonant electrons (5–30 keV) (Figure 9g). As THEMIS A moves progressively toward larger L shells, pronounced pancake distributions (Figure 9h) are frequently observed at low energies (<2 keV), which are associated with the resonance with the upper-band chorus. There is also clear evidence of weak anisotropy and even the existence of slightly inverted population (positive gradient of PSD in energy with $\partial f/\partial E > 0$) at energies around a few keV. Between 1415 and 1424 UT, particle burst data are available in both wave electric and magnetic fields with high frequency and time resolutions (Figure 10), which clearly indicates the intensification of both lower-band and upper-band chorus. Here the intensification of both electric and magnetic fields implies that both lower-band and upper-band chorus are electromagnetic waves during this time interval. At 1423:07 UT, the cyclotron resonant energy for the lower-band chorus (0.2–0.4 f_{ce}) is 10–50 keV, while it decreases to ~2 keV for the upper-band chorus (0.55 f_{ce}), as shown in Figure 9g. At 1423:07 UT, the anisotropy of low-energy (~2 keV) electrons is large enough to produce the upper-band chorus, and the anisotropic distribution of 5–50 keV electrons can produce lower-band chorus. Later, at 1639:13 UT and 1746:29 UT, electron PADs become more isotropic at energies of a few to 50 keV, and chorus waves also become weaker.

6. Summary and Discussions

[25] ESA and SST data from the THEMIS spacecraft have been analyzed to construct a global statistical model of electron pitch angle anisotropy and PSD at various electron energies responsible for the chorus excitation. The main results of our study can be summarized as follows:

[26] 1. Strong chorus waves are confined to regions where the ratio between the plasma frequency and gyrofrequency (f_{pe}/f_{ce}) is less than 5 (with an uncertainty of a factor of ~2). Typically, these regions are found within 7 R_E on the nightside, but extend to 10 R_E in the prenoon sector.

[27] 2. The typical minimum resonant energies for the cyclotron resonance with lower-band chorus waves on the nightside ranges from a few to tens of keV and up to 100 keV on the dayside. Upper-band chorus resonates with electrons at much lower energies between 0.5 and a few keV.

[28] 3. On the nightside, large positive electron anisotropy is only observed at $L < 8$, which is remarkably consistent with the location of intense nightside chorus. Dayside lower-band chorus is generated by cyclotron resonance with 10–100 keV electrons. Such electrons are associated with a less significant flux drop from midnight toward noon, together with a pronounced increase in anisotropy. The combination of these effects produces more frequent and intense dayside chorus generation around 8 R_E in the prenoon sector.

[29] 4. During active geomagnetic conditions, electron PSDs on the nightside increase compared to those at quiet times. Omnidirectional electron PSDs decrease by almost an order of magnitude from midnight through dawn to noon for low-energy electrons (<30 keV) under all geomagnetically disturbed conditions, presumably due to rapid scattering loss through wave-particle interaction. For high-energy electrons (30–100 keV), the electron PSD is essentially independent of MLT, owing to the dominant effect of the magnetic drift compared to loss rates.

[30] 5. Owing to drift shell splitting, electron anisotropy tends to increase at higher energies (10–100 keV) during drift from midnight through dawn to noon. Lower-energy electrons (0.5–2 keV) frequently form pancake distributions in the prenoon sector possibly due to scattering by waves.

[31] 6. The typical energies for the Landau resonance are generally comparable to a few keV, with slightly larger values on the dayside. This energy range is well correlated with a pronounced reduction in anisotropy and slightly inverted population in energy, particularly in the outer dayside magnetosphere. Furthermore, the reduced anisot-

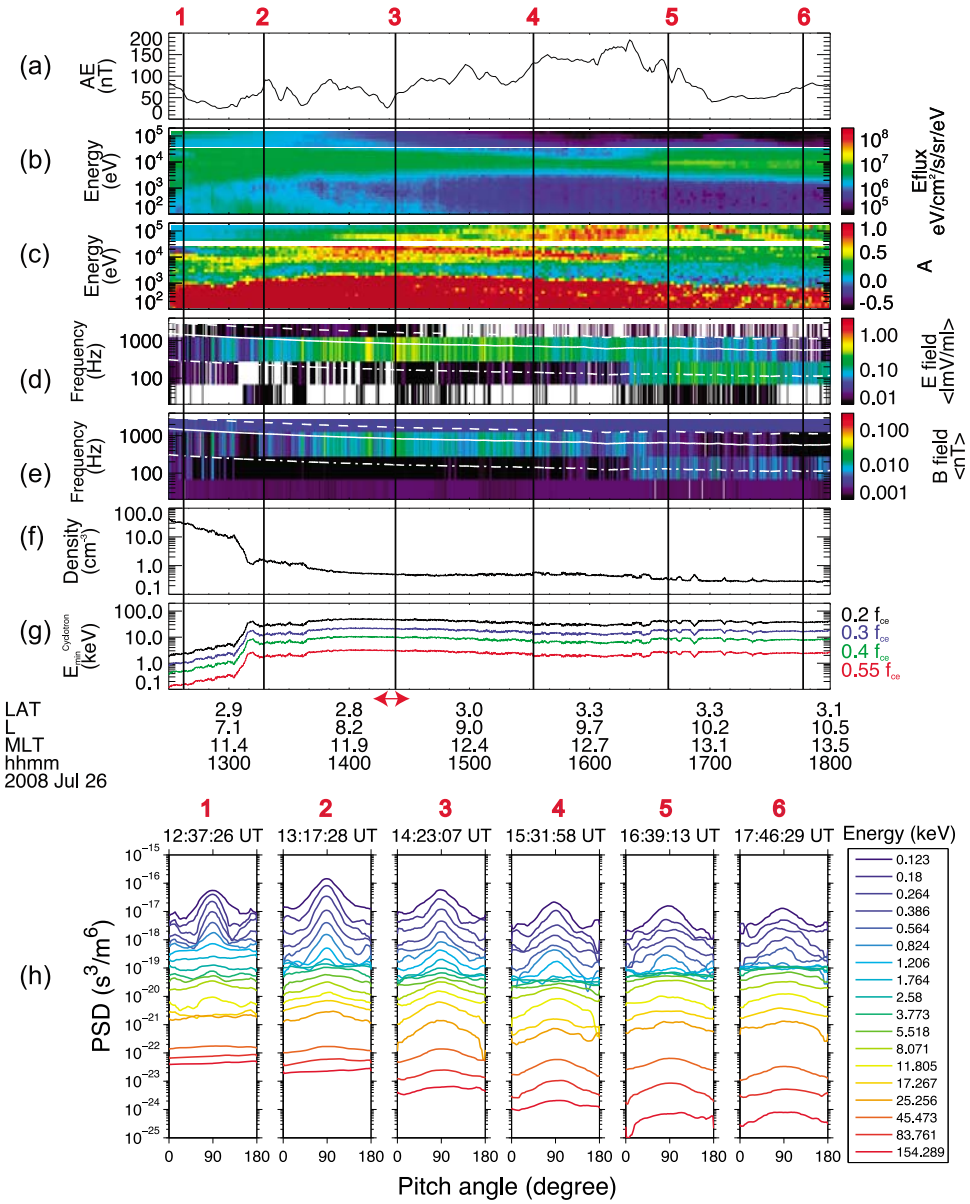

Figure 9. Similar format as Figure 7 but for a dayside event which occurred on 26 July 2008 measured by THEMIS A.

ropy would prevent cyclotron resonant instability in the observed gap near 0.5 f_{ce}.

[32] Pancake distributions are commonly observed in the outer dayside magnetosphere. *Su et al.* [2009] showed that the combination of lower-band and upper-band chorus can effectively scatter electrons with energies of 0.1–2 keV into the loss cone. In the limit of strong diffusion, the diffusion rate is sufficiently large to diffuse particles into the loss cone within less than a bounce period, and the PADs become nearly isotropic at lower pitch angles up to ~60°–70°, thus forming pancake distributions. For weak diffusion, particles are slowly scattered into the loss cone, and the slope of the distribution outside the loss cone is greater than that for the strong diffusion. Interestingly, a slightly inverted energy population is also observed on the dayside for the energies around a few keV. This is possible since high-energy electrons drift faster than low-energy electrons, thus reaching the dayside earlier than the low-energy electrons and forming inverted population. However, distributions with a positive PSD gradient as a function of energy are highly unstable and would be efficiently relaxed once they are formed, leading to the flattened distribution shown in Figure 9h.

[33] For low-energy electrons (<10 keV), omnidirectional electron PSDs drop by almost an order of magnitude from midnight to noon during geomagnetically active times. However, this dropout is mainly due to electrons with low pitch angles scattered by chorus waves, and the PSD for electrons with high pitch angles may not be associated with a significant dropout. Interestingly, *Petrinec et al.* [1999] examined the auroral intensity in X rays as a consequence of energetic electrons (2–25 keV) precipitating into the

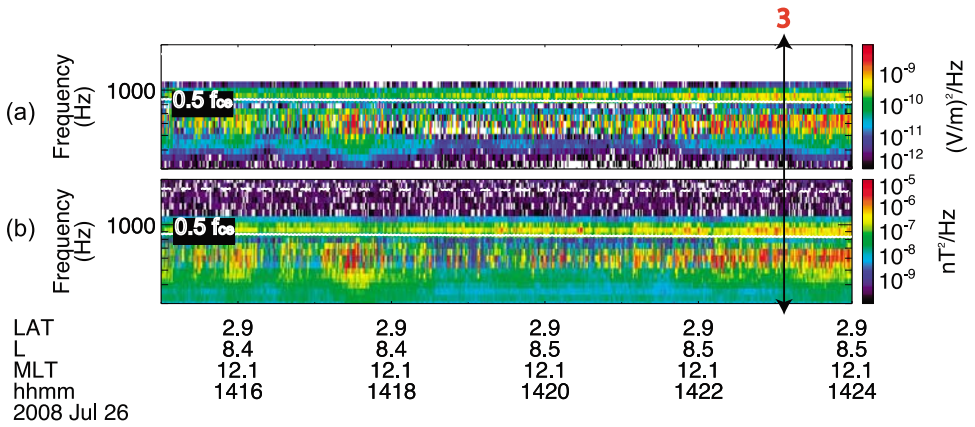

Figure 10. Spectrograms of (a) electric field and (b) magnetic field power spectral densities measured by EFI and SCM (particle burst mode available in the dayside event) in units of $V^2m^{-2}Hz^{-1}$ and nT^2Hz^{-1}. Three white lines indicate equatorial f_{ce} (dashed), 0.5 f_{ce} (solid), and 0.1 f_{ce} (dash-dotted). The black arrow represents the corresponding time when electron distribution data are shown in Figure 9g.

ionosphere at different geomagnetic activities and found that the majority of X ray emissions are observed in the postmidnight sector. The global morphology of X ray emissions is very similar to the electron distribution (2–30 keV) obtained in our study in terms of MLT with a strong dependence on the geomagnetic activity. Therefore precipitations of 2–30 keV electrons scattered by chorus waves may play a significant role in the formation of the diffuse aurora.

[34] In the present study, the minimum resonant energy is calculated based on the assumption that both upper-band and lower-band chorus emissions are electromagnetic waves with small wave normal angles. However, previous studies [e.g., *Goldstein and Tsurutani*, 1984; *Hayakawa et al.*, 1984; *Muto et al.*, 1987; *Hayakawa et al.*, 1989] reported that lower-band chorus is propagating almost exactly along the magnetic field, while upper-band chorus can be highly oblique with wave normal angles close to the resonance cone. On the basis of this analysis of wave normal directions, lower-band chorus is probably excited by the electron cyclotron resonant instability, while upper-band chorus could be excited by a different mechanism. If upper-band chorus is indeed highly oblique, equations (3), (4), and (5), which are used to calculate minimum resonant energies, might not be valid for upper-band chorus. However, upper-band chorus was first detected by search coil magnetometers and an event study reported by *Tsurutani and Smith* [1974] showed that the magnetic field of upper-band chorus is even stronger than that of lower-band chorus, which implies that upper-band chorus is also electromagnetic. With POLAR magnetic field data, strong upper-band chorus comparable to the lower-band chorus emissions is detected both near the equator and midlatitudes [*Lauben et al.*, 1998]. During the dayside event in this paper (Figure 10), the wave spectrum shows comparable intensity in both lower-band and upper-band, and the wave normal angle for both lower-band and upper-band is shown to be within 20° (not explicitly shown in the paper). Investigation of wave normal distributions for lower-band and upper-band chorus is a very interesting but still a controversial topic, which is also extremely important to understand the generation mechanism of lower-band and upper-band chorus. In spite of this limitation, this present study focuses on investigating electron distributions potentially responsible for chorus generation, covering a broad energy range for both electron PSD and anisotropy under different levels of magnetic activity to shed further light on the chorus generation mechanism.

[35] From midnight through dawn to the noon sector, although the plasma density increases, the ratio f_{pe}/f_{ce} becomes smaller due to the dominant effect of increasing electron cyclotron frequencies caused by magnetospheric compression especially at larger L shells. Therefore the minimum resonant energy on the dayside increases up to 100 keV, contrary to the findings from *Åsnes et al.* [2005], who concluded that the minimum resonant energy will be reduced due to an increase in the cold plasma density on the dayside. The assertion of *Åsnes et al.* [2005] could be true at lower L shells (inside geosynchronous orbit), but not at the larger L shells, where chorus is most intense on the dayside.

[36] Previous studies [e.g., *Tsurutani and Smith*, 1977; *Li et al.*, 2009a] showed that the occurrence rate of the dayside chorus is considerably higher than that on the nightside. Statistical results in the present study show that electrons (2–30 keV) on the nightside tend to have a positive anisotropy only during disturbed times associated with injection events, while on the dayside electron anisotropy (10–100 keV) is generally high even during quiet times due to drift shell splitting. Electrons that contribute to the lower-band chorus generation on the dayside have larger minimum resonant energies (10–100 keV). Such electrons are not associated with a significant loss as they drift from midnight toward noon. On the other hand, lower-energy electrons (less than a few keV) responsible for the generation of upper-band chorus on the dayside also generally exhibit large anisotropy due to the resonance with waves during their drift toward the noon sector. The combination of these properties can result in the high occurrence rate of dayside chorus. *Li et al.* [2008, 2009b] simulated path-integrated wave gain along the raypath and showed that

nightside chorus is confined within 15° of the equator due to strong Landau damping. However, previous studies [e.g., *Sazhin and Hayakawa*, 1992; *Meredith et al.*, 2003; *Bortnik et al.*, 2007; *Li et al.*, 2009a] showed that dayside chorus can extend to higher latitudes of 30° or more. In the present study, we found that electron PSDs responsible for the Landau resonance decrease by almost an order of magnitude from midnight through dawn toward the noon sector, which would allow dayside chorus to extend to higher magnetic latitudes due to weaker Landau damping, consistent with *Bortnik et al.* [2007]. The Landau damping on the dayside will be further reduced because of the observed flattening in electron distributions near a few keV. Furthermore, future simulations of the generation of dayside chorus need to include a compressed magnetic field model in order to clearly understand the latitudinal extension of dayside chorus waves.

[37] **Acknowledgments.** This research was funded by NSF grant ATM-0802843, NASA Heliophysics Theory Program grant NNX08A135G, and NASA NAS5–02099. The authors thank World Data Center for Geomagnetism, Kyoto, for providing the *AE* index. Financial support for the work of the FGM Lead Investigator Team at the Technical University of Braunschweig by the German Ministerium für Wirtschaft und Technologie and the Deutsches Zentrum für Luft-und Raumfahrt under grant 50QP0402 is acknowledged.

[38] Amitava Bhattacharjee thanks the reviewers for their assistance in evaluating this paper.

References

Albert, J. M. (2005), Evaluation of quasi-linear diffusion coefficients for whistler mode waves in a plasma with arbitrary density ratio, *J. Geophys. Res.*, *110*, A03218, doi:10.1029/2004JA010844.

Anderson, R. R., and K. Maeda (1977), VLF emissions associated with enhanced magnetospheric electrons, *J. Geophys. Res.*, *82*(1), 135–146, doi:10.1029/JA082i001p00135.

Angelopoulos, V. (2008), The THEMIS mission, *Space Sci. Rev.*, *141*(1–4), 5–34, doi:10.1007/s11214-008-9336-1.

Åsnes, A., R. W. Friedel, J. Stadsnes, M. Thomsen, N. Østgaard, and T. Cayton (2005), Statistical pitch angle properties of substorm-injected electron clouds and their relation to dawnside energetic electron precipitation, *J. Geophys. Res.*, *110*, A05207, doi:10.1029/2004JA010838.

Auster, H. U., et al. (2008), The THEMIS fluxgate magnetometer, *Space Sci. Rev.*, doi:10.1007/s11214-008-9365-9.

Bell, T. F., U. S. Inan, N. Haque, and J. S. Pickett (2009), Source regions of banded chorus, *Geophys. Res. Lett.*, *36*, L11101, doi:10.1029/2009GL037629.

Bonnell, J. W., F. S. Mozer, G. T. Delory, A. J. Hull, R. E. Ergun, C. M. Cully, V. Angelopoulos, and P. R. Harvey (2008), The Electric Field Instrument (EFI) for THEMIS, *Space Sci. Rev.*, *141*, 303–341, doi:10.1007/s11214-008-9469-2.

Bortnik, J., R. M. Thorne, and N. P. Meredith (2007), Modeling the propagation characteristics of chorus using CRRES suprathermal electron fluxes, *J. Geophys. Res.*, *112*, A08204, doi:10.1029/2006JA012237.

Breneman, A. W., C. A. Kletzing, J. Pickett, J. Chum, and O. Santolik (2009), Statistics of multispacecraft observations of chorus dispersion and source location, *J. Geophys. Res.*, *114*, A06202, doi:10.1029/2008JA013549.

Burtis, W. J., and R. A. Helliwell (1969), Banded chorus: A new type of VLF radiation observed in the magnetosphere by OGO 1 and OGO 3, *J. Geophys. Res.*, *74*(11), 3002–3010, doi:10.1029/JA074i011p03002.

Burton, R. K., and R. E. Holzer (1974), The origin and propagation of chorus in the outer magnetosphere, *J. Geophys. Res.*, *79*(7), 1014–1023, doi:10.1029/JA079i007p01014.

Chen, M. W., and M. Schulz (2001a), Simulations of storm time diffuse aurora with plasmasheet electrons in strong pitch angle diffusion, *J. Geophys. Res.*, *106*(A2), 1873–1886, doi:10.1029/2000JA000161.

Chen, M. W., and M. Schulz (2001b), Simulations of diffuse aurora with plasma sheet electrons in pitch angle diffusion less than everywhere strong, *J. Geophys. Res.*, *106*(A12), 28,949–28,966, doi:10.1029/2001JA000138.

Chen, M. W., J. L. Roeder, J. F. Fennell, L. R. Lyons, R. L. Lambour, and M. Schulz (1999), Proton ring current pitch angle distributions: Comparison of simulations with CRRES observations, *J. Geophys. Res.*, *104*(A8), 17,379–17,389, doi:10.1029/1999JA900142.

Chum, J., O. Santolik, A. W. Breneman, C. A. Kletzing, D. A. Gurnett, and J. S. Pickett (2007), Chorus source properties that produce time shifts and frequency range differences observed on different Cluster spacecraft, *J. Geophys. Res.*, *112*, A06206, doi:10.1029/2006JA012061.

Cully, C.M., R. E. Ergun, K. Stevens, A. Nammari, and J. Westfall (2008), The THEMIS digital fields board, *Space Sci. Rev.*, *141*(1–4), 343–355, doi:10.1007/s11214-008-9417-1.

Denton, M. H., M. F. Thomsen, H. Korth, S. Lynch, J. C. Zhang, and M. W. Liemohn (2005), Bulk plasma properties at geosynchronous orbit, *J. Geophys. Res.*, *110*, A07223, doi:10.1029/2004JA010861.

Goldstein, B. E., and B. T. Tsurutani (1984), Wave normal directions of chorus near the equatorial source region, *J. Geophys. Res.*, *89*(A5), 2789–2810, doi:10.1029/JA089iA05p02789.

Hashimoto, K., and I. Kimura (1981), A generation mechanism of narrow band hiss emissions above one half the electron cyclotron frequency in the outer magnetosphere, *J. Geophys. Res.*, *86*(A13), 11,148–11,152, doi:10.1029/JA086iA13p11148.

Hayakawa, M., Y. Yamanaka, M. Parrot, and F. Lefeuvre (1984), The wave normals of magnetospheric chorus emissions observed on board GEOS 2, *J. Geophys. Res.*, *89*(A5), 2811–2821, doi:10.1029/JA089iA05p02811.

Hayakawa, M., H. Muto, S. Shimakura, K. Hattori, M. Parrot, and F. Lefeuvre (1989), The wave normal direction of chorus emissions in the outer magnetosphere, *Proc. NIPR Symp. Upper Atmos. Phys.*, *2*, 62–73.

Horne, R. B., and R. M. Thorne (2003), Relativistic electron acceleration and precipitation during resonant interactions with whistler-mode chorus, *Geophys. Res. Lett.*, *30*(10), 1527, doi:10.1029/2003GL016973.

Horne, R. B., R. M. Thorne, N. P. Meredith, and R. R. Anderson (2003a), Diffuse auroral electron scattering by electron cyclotron harmonic and whistler mode waves during an isolated substorm, *J. Geophys. Res.*, *108*(A7), 1290, doi:10.1029/2002JA009736.

Horne, R. B., N. P. Meredith, R. M. Thorne, D. Heynderickx, R. H. A. Iles, and R. R. Anderson (2003b), Evolution of energetic pitch angle distributions during storm-time electron acceleration to megaelectronvolt energies, *J. Geophys. Res.*, *108*(A1), 1016, doi:10.1029/2001JA009165.

Horne, R. B., R. M. Thorne, S. A. Glauert, J. M. Albert, N. P. Meredith, and R. R. Anderson (2005), Timescales for radiation belt electron acceleration by whistler mode chorus, *J. Geophys. Res.*, *110*, A03225, doi:10.1029/2004JA010811.

Isenberg, P. A., H. C. Koons, and J. F. Fennell (1982), Simultaneous observations of energetic electrons and dawnside chorus in geosynchronous orbit, *J. Geophys. Res.*, *87*(A3), 1495–1503, doi:10.1029/JA087iA03p01495.

Katoh, Y., and Y. Omura (2007a), Computer simulation of chorus wave generation in the Earth's inner magnetosphere, *Geophys. Res. Lett.*, *34*, L03102, doi:10.1029/2006GL028594.

Katoh, Y., and Y. Omura (2007b), Relativistic particle acceleration in the process of whistler-mode chorus wave generation, *Geophys. Res. Lett.*, *34*, L13102, doi:10.1029/2007GL029758.

Kennel, C. F. (1966), Low frequency whistler mode, *Phys. Fluids*, *9*, 2190, doi:10.1063/1.1761588.

Kennel, C. F., and H. E. Petschek (1966), Limit on stable trapped particle fluxes, *J. Geophys. Res.*, *71*, 1–28.

Kennel, C. F., and R. M. Thorne (1967), Unstable growth of unducted whistlers propagating at an angle to the geomagnetic field, *J. Geophys. Res.*, *72*(3), 871–878, doi:10.1029/JZ072i003p00871.

Koons, H. C., and J. L. Roeder (1990), A survey of equatorial magnetospheric wave activity between 5 and 8 R_E, *Planet. Space Sci.*, *38*(10), 1335–1341, doi:10.1016/0032-0633(90)90136-E.

Korth, H., M. F. Thomsen, J. E. Borovsky, and D. J. McComas (1999), Plasma sheet access to geosynchronous orbit, *J. Geophys. Res.*, *104*(A11), 25,047–25,061, doi:10.1029/1999JA900292.

Lauben, D. S., U. S. Inan, T. F. Bell, D. L. Kirchner, G. B. Hospodarsky, and J. S. Pickett (1998), VLF chorus emissions observed by Polar during the January 10, 1997, magnetic cloud, *Geophys. Res. Lett.*, *25*(15), 2995–2998, doi:10.1029/98GL01425.

Lauben, D. S., U. S. Inan, T. F. Bell, and D. A. Gurnett (2002), Source characteristics of ELF/VLF chorus, *J. Geophys. Res.*, *107*(A12), 1429, doi:10.1029/2000JA003019.

Le Contel, O., et al. (2008), First results of the THEMIS searchcoil magentometers, *Space Sci. Rev.*, *141*, 509–534, doi:10.1007/s11214-008-9371-y.

LeDocq, M. J., D. A. Gurnett, and G. B. Hospodarsky (1998), Chorus source locations from VLF Poynting flux measurements with the Polar spacecraft, *Geophys. Res. Lett.*, *25*(21), 4063–4066, doi:10.1029/1998GL900071.

Li, W., Y. Y. Shprits, and R. M. Thorne (2007), Dynamic evolution of energetic outer zone electrons due to wave-particle interactions during storms, *J. Geophys. Res.*, *112*, A10220, doi:10.1029/2007JA012368.

Li, W., R. M. Thorne, N. P. Meredith, R. B. Horne, J. Bortnik, Y. Y. Shprits, and B. Ni (2008), Evaluation of whistler mode chorus amplification during an injection event observed on CRRES, *J. Geophys. Res.*, *113*, A09210, doi:10.1029/2008JA013129.

Li, W., R. M. Thorne, V. Angelopoulos, J. Bortnik, C. M. Cully, B. Ni, O. LeContel, A. Roux, U. Auster, and W. Magnes (2009a), Global distribution of whistler-mode chorus waves observed on the THEMIS spacecraft, *Geophys. Res. Lett.*, *36*, L09104, doi:10.1029/2009GL037595.

Li, W., R. M. Thorne, V. Angelopoulos, J. W. Bonnell, J. P. McFadden, C. W. Carlson, O. LeContel, A. Roux, K. H. Glassmeier, and H. U. Auster (2009b), Evaluation of whistler-mode chorus intensification on the nightside during an injection event observed on the THEMIS spacecraft, *J. Geophys. Res.*, *114*, A00C14, doi:10.1029/2008JA013554.

Lyons, L. R., R. M. Thorne, and C. F. Kennel (1972), Pitch-angle diffusion of radiation belt electrons within the plasmasphere, *J. Geophys. Res.*, *77*(19), 3455–3474, doi:10.1029/JA077i019p03455.

McFadden, J. P., C. W. Carlson, D. Larson, V. Angelopoulos, M. Ludlam, R. Abiad, B. Elliott, P. Turin, and M. Marckwordt (2008), The THEMIS ESA plasma instrument and in-flight calibration, *Space Sci. Rev.*, *141*, 277–302, doi:10.1107/s11214-008-9440-2.

Meredith, N. P., A. D. Johnstone, S. Szita, R. B. Horne, and R. R. Anderson (1999), "Pancake" electron distributions in the outer radiation belts, *J. Geophys. Res.*, *104*(A6), 12,431–12,444, doi:10.1029/1998JA900083.

Meredith, N. P., R. B. Horne, and R. R. Anderson (2001), Substorm dependence of chorus amplitudes: Implications for the acceleration of electrons to relativistic energies, *J. Geophys. Res.*, *106*(A7), 13,165–13,178, doi:10.1029/2000JA900156.

Meredith, N. P., R. B. Horne, R. H. A. Iles, R. M. Thorne, D. Heynderickx, and R. R. Anderson (2002), Outer zone relativistic electron acceleration associated with substorm-enhanced whistler mode chorus, *J. Geophys. Res.*, *107*(A7), 1144, doi:10.1029/2001JA900146.

Meredith, N. P., R. B. Horne, R. M. Thorne, and R. R. Anderson (2003), Favored regions for chorus-driven electron acceleration to relativistic energies in the Earth's outer radiation belt, *Geophys. Res. Lett.*, *30*(16), 1871, doi:10.1029/2003GL017698.

Meredith, N. P., R. B. Horne, R. M. Thorne, and R. R. Anderson (2009), Survey of upper band chorus and ECH waves: Implications for the diffuse aurora, *J. Geophys. Res.*, *114*, A07218, doi:10.1029/2009JA014230.

Miyoshi, Y., A. Morioka, H. Misawa, T. Obara, T. Nagai, and Y. Kasahara (2003), Rebuilding process of the outer radiation belt during the 3 November 1993 magnetic storm: NOAA and Exos-D observations, *J. Geophys. Res.*, *108*(A1), 1004, doi:10.1029/2001JA007542.

Miyoshi, Y., A. Morioka, R. Kataoka, Y. Kasahara, and T. Mukai (2007), Evolution of the outer radiation belt during the November 1993 storms driven by corotating interaction regions, *J. Geophys. Res.*, *112*, A05210, doi:10.1029/2006JA012148.

Moldwin, M. B., M. F. Thomsen, S. J. Bame, D. J. McComas, and K. R. Moore (1994), An examination of the structure and dynamics of the outer plasmasphere using multiple geosynchronous satellites, *J. Geophys. Res.*, *99*(A6), 11,475–11,481, doi:10.1029/93JA03526.

Mozer, F. S. (1973), Analysis of techniques for measuring DC and AC electric fields in the magnetosphere, *Space Sci. Rev.*, *14*(2), 272–313, doi:10.1007/BF02432099.

Muto, H., M. Hayakawa, M. Parrot, and F. Lefeuvre (1987), Direction finding of half-gyrofrequency VLF emissions in the off-equatorial region of the magnetosphere and their generation and propagation, *J. Geophys. Res.*, *92*(A7), 7538–7550, doi:10.1029/JA092iA07p07538.

Ni, B., R. M. Thorne, Y. Y. Shprits, and J. Bortnik (2008), Resonant scattering of plasma sheet electrons by whistler-mode chorus: Contribution to diffuse auroral precipitation, *Geophys. Res. Lett.*, *35*, L11106, doi:10.1029/2008GL034032.

Nunn, D., Y. Omura, H. Matsumoto, I. Nagano, and S. Yagitani (1997), The numerical simulation of VLF chorus and discrete emissions observed on the Geotail satellite using a Vlasov code, *J. Geophys. Res.*, *102*(A12), 27,083–27,098, doi:10.1029/97JA02518.

Omura, Y., Y. Katoh, and D. Summers (2008), Theory and simulation of the generation of whistler-mode chorus, *J. Geophys. Res.*, *113*, A04223, doi:10.1029/2007JA012622.

Parrot, M., O. Santolik, N. Cornilleau-Wehrlin, M. Maksimovic, and C. Harvey (2003), Source location of chorus emissions observed by CLUSTER, *Ann. Geophys.*, *21*, 473–480.

Pedersen, A., F. Mozer, and G. Gustafsson (1998), Electric field measurements in a tenuous plasma with spherical double probes, in *Measurement Techniques in Space Plasmas: Fields*, *Geophys. Monogr. Ser.*, vol. 103, edited by J. Borovsky, R. Pfaff, and A. Young, pp. 1–12, AGU, Washington, D. C.

Petrinec, S. M., D. L. Chenette, J. Mobilia, M. A. Rinaldi, and W. L. Imhof (1999), Statistical X ray auroral emissions–PIXIE observations, *Geophys. Res. Lett.*, *26*(11), 1565–1568, doi:10.1029/1999GL900295.

Roederer, J. G. (1967), On the adiabatic motion of energetic particles in a model magnetosphere, *J. Geophys. Res.*, *72*(3), 981–992, doi:10.1029/JZ072i003p00981.

Roederer, J. G., and M. Schulz (1969), Effect of shell splitting on radial diffusion in the magnetosphere, *J. Geophys. Res.*, *74*(16), 4117–4122, doi:10.1029/JA074i016p04117.

Roux, A., O. Le Contel, C. Coillot, A. Bouabdellah, B. de la Porte, D. Alison, S. Ruocco, and M. C. Vassal (2008), The search coil magnetometer for THEMIS, *Space Sci. Rev.*, *141*, 265–275, doi:10.1007/s11214-008-9455-8.

Santolík, O., D. A. Gurnett, J. S. Pickett, M. Parrot, and N. Cornilleau-Wehrlin (2003), Spatio-temporal structure of storm-time chorus, *J. Geophys. Res.*, *108*(A7), 1278, doi:10.1029/2002JA009791.

Santolik, O., E. Macusova, K. H. Yearby, N. Cornilleau-Wehrlin, and H. SC. K. Alleyne (2005), Radial variation of whistler-mode chorus: First results from the STAFF/DWP instrument onboard the Double Star TC 1 spacecraft, *Ann. Geophys.*, *23*, 2937–2942.

Sazhin, S. S., and M. Hayakawa (1992), Magnetospheric chorus emissions: A review, Planet. Space Sci., *40*, 681–697, doi:10.1016/0032-0633(92)90009-D.

Sheeley, B. W., M. B. Moldwin, H. K. Rassoul, and R. R. Anderson (2001), An empirical plasmasphere and trough density model: CRRES observations, *J. Geophys. Res.*, *106*(A11), 25,631–25,641, doi:10.1029/2000JA000286.

Shprits, Y. Y., N. P. Meredith, and R. M. Thorne (2007), Parameterization of radiation belt electron loss timescales due to interactions with chorus waves, *Geophys. Res. Lett.*, *34*, L11110, doi:10.1029/2006GL029050.

Sibeck, D. G., R. W. McEntire, A. T. Y. Lui, R. E. Lopez, and S. M. Krimigis (1987), Magnetic field drift shell splitting: Cause of unusual dayside particle pitch angle distributions during storms and substorms, *J. Geophys. Res.*, *92*(A12), 13,485–13,497, doi:10.1029/JA092iA12p13485.

Stix, T. H. (1962), *The Theory of Plasma Waves*, McGraw-Hill, New York.

Su, Z., H. Zheng, and S. Wang (2009), Evolution of electron pitch angle distribution due to interactions with whistler mode chorus following substorm injections, *J. Geophys. Res.*, *114*, A08202, doi:10.1029/2009JA014269.

Summers, D., and R. M. Thorne (2003), Relativistic electron pitch-angle scattering by electromagnetic ion cyclotron waves during geomagnetic storms, *J. Geophys. Res.*, *108*(A4), 1143, doi:10.1029/2002JA009489.

Summers, D., C. Ma, N. P. Meredith, R. B. Horne, R. M. Thorne, D. Heynderickx, and R. R. Anderson (2002), Model of the energization of outer-zone electrons by whistler-mode chorus during the October 9, 1990 geomagnetic storm, *Geophys. Res. Lett.*, *29*(24), 2174, doi:10.1029/2002GL016039.

Thorne, R. M., R. B. Horne, S. Glauert, N. Meredith, Y. Y. Shprits, D. Summers, and R. Anderson (2005), The influence of wave-particle interactions on relativistic electron dynamics during storms, in *Inner Magnetosphere Interaction: New Perspectives From Imaging*, *Geophys. Monogr. Ser.*, vol. 159, edited by J. Burch, M. Schulz, and H. Spence, pp. 101–112, AGU, Washington, D. C.

Thorne, R. M., Y. Y. Shprits, N. P. Meredith, R. B. Horne, W. Li, and L. R. Lyons (2007), Refilling of the slot region between the inner and outer electron radiation belts during geomagnetic storms, *J. Geophys. Res.*, *112*, A06203, doi:10.1029/2006JA012176.

Tsurutani, B. T., and E. J. Smith (1974), Postmidnight chorus: A substorm phenomenon, *J. Geophys. Res.*, *79*(1), 118–127, doi:10.1029/JA079i001p00118.

Tsurutani, B. T., and E. J. Smith (1977), Two types of magnetospheric ELF chorus and their substorm dependencies, *J. Geophys. Res.*, *82*(32), 5112–5128, doi:10.1029/JA082i032p05112.

Tsurutani, B. T., E. J. Smith, H. I. West, and R. M. Buck (1979), Chorus, energetic electrons and magnetospheric substorms, in *Wave Instabilities in Space Plasmas*, edited by P. J. Palmadesso and K. Papadopoulos, pp. 55–62, D. Reidel, Hingham, Mass.

Tsurutani, B. T., O. P. Verkhoglyadova, G. S. Lakhina, and S. Yagitani (2009), Properties of dayside outer zone chorus during HILDCAA events: Loss of energetic electrons, *J. Geophys. Res.*, *114*, A03207, doi:10.1029/2008JA013353.

Tsyganenko, N. A., and D. P. Stern (1996), Modeling the global magnetic field of the large-scale Birkeland current systems, *J. Geophys. Res.*, *101*(A12), 27,187–27,198, doi:10.1029/96JA02735.

Vaivads, A., O. Santolík, G. Stenberg, M. André, C. J. Owen, P. Canu, and M. Dunlop (2007), Source of whistler emissions at the dayside magnetopause, *Geophys. Res. Lett.*, *34*, L09106, doi:10.1029/2006GL029195.

West, H. I., Jr., R. M. Buck, and J. R. Walton (1973), Electron pitch angle distributions throughout the magnetosphere as observed on OGO 5, *J. Geophys. Res.*, *78*(7), 1064–1081, doi:10.1029/JA078i007p01064.

V. Angelopoulos, Institute of Geophysics and Planetary Physics, Department of Earth and Space Sciences, University of California, Los Angeles, CA 90095-1567, USA. (vassilis@ucla.edu)

U. Auster, Institut für Geophysik und extraterrestrische Physik, Technischen Universität Braunschweig, Mendelssohnstrasse 3, D-38106 Braunschweig, Germany. (uli.auster@tu-braunschweig.de)

J. W. Bonnell, D. E. Larson, and J. P. McFadden, Space Sciences Laboratory, University of California, 7 Gauss Way, Berkeley, CA 94720-7450, USA. (jbonnell@ssl.berkeley.edu; davin@ssl.berkeley.edu; mcfadden@ssl.berkeley.edu)

J. Bortnik, W. Li, Y. Nishimura, and R. M. Thorne, Department of Atmospheric and Oceanic Sciences, University of California, 405 Hilgard Avenue, Los Angeles, CA 90095-1565, USA. (jbortnik@gmail.com; moonli@atmos.ucla.edu; toshi@atmos.ucla.edu; rmt@atmos.ucla.edu)

O. Le Contel and A. Roux, Laboratoire de Physique des Plasmas, Ecole Polytechnique, Route de Saclay, F-91128 Palaiseau CEDEX, France. (olivier.lecontel@lpp.polytechnique.fr; alain.roux@lpp.polytechnique.fr)